Structures, Jet-and-Crossflow Interactions, and Cross-plane Entrainment Mechanism of a Jet in Crossflow

Kwanmon Sornphrom and Asi Bunyajitradulya*

Department of Mechanical Engineering, Faculty of Engineering, Chulalongkorn University, Bangkok 10330, Thailand
* Corresponding Author: E-mail: asi.b@chula.ac.th, Tel: 02 218 6645, Fax: 02 218 6645

Abstract

Structures, jet-and-crossflow interactions, entrainment, and cross-plane entrainment mechanism of a jet in crossflow are investigated. Stereoscopic Particle Image Velocimetry together with both jet-fluid only and jet-and-crossflow fluid seeding schemes are used. The experiment is conducted at the jet-to-crossflow effective velocity ratio (r) of 4 and the crossflow Reynolds number (Re_{cf}) of 3,100. The results on jet structures, jet-and-crossflow interactions, and especially cross-plane entrainment mechanism can be summarized in three subsequent stages as follows. 1) Jet-CVP-induced pure crossflow vortical motion: Pure crossflow fluid from each lateral side of the jet is induced and brought towards the bell-shaped inlet of the converging-diverging vertical channel of high upward flow at the bottom edge of the jet. 2) Jet-CVP-induced converging-diverging vertical channel of high upward flow: The pure crossflow fluid at the bottom edge of the jet below and around the bell-shaped inlet is subsequently entrained continuously but intensely in the upstream portion of the converging section of the channel. The intensity of entrainment in the upstream portion of the converging section is such that, when the fluid reaches the throat of the channel at the center of the gulf region of the jet kidney-shaped structure, it already becomes mostly jet-fluid mixture. 3) Free-jet like entrainment by the jet kidney-shaped structure: The jet-fluid mixture in the gulf region of low streamwise velocity is further entrained into the jet kidney-shaped structure of high streamwise jet velocity, similar to free-jet entrainment.

***Keywords**:* jet in crossflow, entrainment, mechanism, counter-rotating vortex pair (CVP)

1. Introduction

Jet in crossflow (JICF) is a flow in which a jet is normally injected into crossflow. As the jet penetrates into the crossflow, it interacts with the crossflow, resulting in the bending of the jet in the crossflow direction and various vortical structures. The interactions and vortical structures in turn result in specific flow characteristics such as entrainment and trajectory. These characteristics are important in many engineering applications such as fuel injection in a combustion chamber, industrial smoke stack, Vertical Short Take Off and Landing (V/STOL), and film cooling technique on turbine blades.

While our earlier works (see, e.g., Witayaprapakorn and Bunyajitradulya [1], Chaikasetsin *et al.* [2], Bunyajitradulya [3], and Wangkiat *et al*. [4]) attempts to address the issue of determining the volumetric entrainment ratio (E) more directly, in this work we continue to attempt to address the issue of entrainment mechanism of JICF. In this regard, Yuan and Street [5], see also Yuan *et al.* [6], suggested that in the jet bending region JICF entrainment is enhanced by the engulfment of crossflow fluid into the large gap formed at the upstream edge of the jet. This gap is the result of the interaction between upstream and downstream spanwise rollers. As for the role of the CVP in entrainment, they observed that although the mean circulation of the CVP is weak, it does help increasing the surface area of the jet, which results in entrainment enhancement. Cortelezzi and Karagozian [7], using three-dimensional vortex element, found that JICF entrainment is due to the incoming upstream crossflow being deflected about the jet, lifted up on the lee side of the jet into the center region between the CVP, and subsequently wound into the CVP. Sau *et al*. [8] found that the tails of the upstream horseshoe vortical structures as well as the surrounding incoming floor shear layer are lifted up from the floor on the lee side of the jet and subsequently entrained into the CVP.

While these numerical simulation works have shed lights on various aspects of entrainment mechanism of JICF, empirical evidences are still rare. In the present work, we therefore attempt to

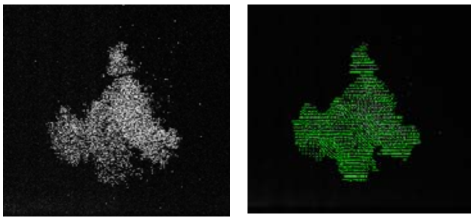

(a) Jet-fluid only seeding.

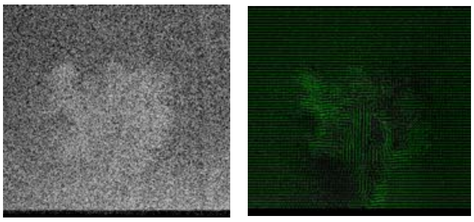

(b) Jet-and-crossflow fluid seeding.

Fig. 1. Comparison of instantaneous particle images (left) and the corresponding processed instantaneous vector fields (right) between
(a) jet-fluid only seeding, and
(b) jet-and-crossflow fluid seeding.

address this issue. In order to determine the volumetric entrainment ratio (E) of a jet in crossflow more directly, the planar velocity field information from Stereoscopic Particle Image Velocimetry (SPIV) together with the jet-fluid only seeding scheme is required. However, in order to investigate the structures, jet-and-crossflow interactions, and cross-plane entrainment mechanism of a jet in crossflow more clearly, additional information on the planar velocity field from SPIV with both jet-and-crossflow fluid seeding scheme is required. Therefore, in the present work SPIV with both seeding schemes are employed. The experimented is conducted for JICF with effective velocity ratio (r) of 4; the jet Reynolds numbers (Re_j) of 12,400; and a crossflow Reynolds number (Re_{cf}) of 3,100.

2. Experimental Principles and Techniques

First, we introduce the coordinate system employed in this work (shown in Fig. 2): the origin of the coordinate system is at the center of the jet at the jet exit plane; x, y, and z are the streamwise (crossflow direction), traverse (main jet direction at the jet exit), and spanwise coordinates, respectively; t is time. Note that the spatial vector from the origin is denoted by $\vec{x} = (x, y, z)$ while x is simply the coordinate along the crossflow direction.

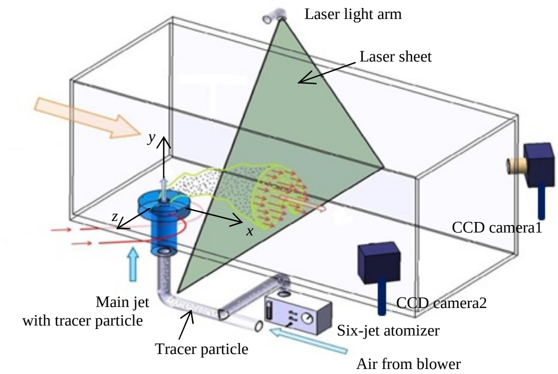

Fig. 2. The test rig and the SPIV setup (Chaikasetsin *et al.* [2]).

As described in Sec. 1, in this work we are required to use SPIV with both seeding schemes. In this section, we briefly summarized the two seeding schemes.

2.1. SPIV with jet-fluid only seeding scheme

The principle of the experimental technique of using SPIV with jet-fluid only - and not the crossflow fluid - seeding scheme to determine entrainment is described in Witayaprapakorn and Bunyajitradulya [1], and Chaikasetsin *et al.* [2] (see also Bunyajitradulya [3], and Wangkiat *et al.* [4]). The reader is therefore referred to these works. Briefly, though, with the SPIV with the jet-fluid only seeding scheme, we can instantaneously and clearly identify and differentiate the region of the jet-fluid mixture from the surrounding pure crossflow fluid at a jet cross section as illustrated in Fig. 1(a). Hence, the SPIV registers only the jet-fluid mixture velocity over the jet-fluid mixture cross section. In the surrounding pure crossflow region, the SPIV registers zero velocity since there are no PIV tracer particles. We shall refer to this planar velocity field acquired from this seeding scheme as the *jet velocity*, $\vec{V}_j(\vec{x},t)$. With this instantaneous jet velocity field, the instantaneous jet volume flowrate at a cross plane cross section at x and time t, $Q_j(x,t)$, and consequently the corresponding time-mean jet volume flowrate through the cross plane at x, $Q_j(x)$, can be found. Finally, the time-mean volumetric entrainment ratio E can be found from

$$E(x) = \frac{Q_j(x)}{Q_o}, \qquad (1)$$

where Q_o is the initial jet volume flowrate at the jet exit.

2.2. SPIV with both jet-and-crossflow fluid seeding scheme

When both jet and crossflow fluids are seeded, SPIV registers the instantaneous *field velocity* $\bar{V}(\vec{x},t)$. That is, at a space-time point $(\vec{x},t)$, the SPIV registers *a* velocity, regardless of whether the jet-fluid mixture or the pure crossflow fluid presently occupies that point. This is illustrated in Fig. 1(b).

2.3. Investigation of entrainment mechanism

For the investigation of the interactions between the jet and the crossflow and, particularly, the entrainment mechanism, the data and results from both cases of seeding: jet-fluid only, and jet-and-crossflow fluid seeding schemes, need to be taken into account and analyzed together. In this case, since it is not yet possible with the current setup to acquire both types of data from both types of seeding *simultaneously*, each case of seeding has to be done at two different times, or *realizations*. As a result, we find for each case of seeding, or each realization:

- Jet-fluid only seeding, realization ω:
  The time-mean jet velocity: $V_{j,\omega}$
- Jet-and-crossflow fluid seeding, realization ω':
  The time-mean field velocity: $V_{\omega'}$

For any realization ω', the time-mean field velocity $V_{\omega'}$ can be written as the sum of the time-mean jet velocity $V_{j,\omega'}$ and the time-mean pure crossflow velocity $V_{cf,\omega'}$ of that realization according to

$$V_{\omega'} = \frac{1}{N}\sum_{n=1}^{N} V_{n,\omega'} = \frac{1}{N}\left[\sum_{n_j=1}^{N_j} V_{j,n_j,\omega'} + \sum_{n_{cf}=1}^{N_{cf}} V_{cf,n_{cf},\omega'}\right]$$
$$= V_{j,\omega'} + V_{cf,\omega'}$$

where $N = N_j + N_{cf}$, and n_j and N_j are the index for and the total number of snapshots that the jet-fluid mixture is present at that point, and n_{cf} and N_{cf} are the index for and the total number of snapshots that the pure crossflow is present at that point.

Hence, when we subtract the time-mean jet velocity from the time-mean field velocity from the two realizations, we have

$$V_{\omega'} - V_{j,\omega} = V_{cf,\omega'} + (V_{j,\omega'} - V_{j,\omega}).$$

If the flow is steady-in-mean and the time period of taking average is sufficiently long enough, we have $V_{j,\omega'} \approx V_{j,\omega}$. Thus, we can approximate the time-mean crossflow velocity as the difference between the time-means above:

$$V_{cf,\omega'} \approx V_{\omega'} - V_{j,\omega}. \qquad (2)$$

For convenience in referencing, we shall simply refer to the derived time-mean crossflow velocity as calculated from Eq. (2) as the time-mean crossflow velocity.

3. Experimental Setup

3.1. Experimental apparatus

The experimental setup is shown in Fig. 2 (Chaikasetsin *et al.* [2]), including the reference coordinate system. The setup is basically identical to that of Wangkiat *et al.* [4], which is slightly modified from Chaikasetsin *et al.* [2]; it is briefly summarized here. The crossflow is generated in the 50×50 cm^2 test section of the open-circuit blower-type wind tunnel. For the main jet assembly, the main jet has an inner diameter (d) of 12.57 mm, and there is a 77d long straight pipe section leading to the main jet exit in order to ensure the fully-developed turbulent pipe flow velocity profile at the jet exit. Note that, unlike Wangkiat *et al.*, this work focuses on JICF only and not controlled JICF (cJICF), therefore azimuthal control jets are not activated. Instead, in addition to jet-fluid only seeding scheme, this work also requires the case of jet-and-crossflow fluid seeding in order to investigate the entrainment mechanism.

3.2. Stereo particle image velocimetry (SPIV)

In this experiment, Stereo Particle Image Velocimetry (SPIV) is used to measure all three components of the velocity vector (V_x, V_y, V_z) in a cross plane. It is basically the same TSI™ SPIV system as used in Wangkiat *et al.* [4]. The tracer particles are 5% by volume glycerol solution for jet-fluid seeding, which is introduced into the pipe far upstream from the main jet exit to ensure particle uniformity before the jet exit. The tracer particles are 50% by volume glycerol solution for crossflow-fluid seeding, which is introduced at the wind tunnel blower inlet. The particle images are captured and analyzed, and the instantaneous velocity field snapshots are rendered by TSI™ Insight 4G program. The instantaneous velocity field snapshots are then further analyzed by in-house program.

For the present results, the three-dimension velocity field snapshots are collected at the rate of 2.07 Hz for a total of 2,000 snapshots. The spatial resolution of the velocity fields ranges from

0.965×0.965 mm^2 at x/rd = 0.5 to 0.935×0.935 mm^2 at x/rd = 1.5. The time-mean velocity field has approximately 5,000 to 13,000 vectors.

3.3. Experimental condition and scope

The experiment is conducted for JICF with the jet-to-crossflow effective velocity ratio r of 4. Note that the effective velocity ratio r is defined as the square root of the jet-to-crossflow momentum flux ratio,

$$r = \sqrt{\rho_j u_j^2 / \rho_{cf} u_{cf}^2}\,, \qquad (3)$$

where ρ is density, u is velocity, and subscripts j and cf refer to jet and the crossflow, respectively. For the jet velocity u_j, the area-averaged jet velocity at the jet exit is used and is equal to 16.3 m/s, while u_{cf} is at 4.0 m/s. This results in the jet Reynolds numbers Re_j of 12,400, and a crossflow Reynolds number Re_{cf} of 3,100. Note that the jet and crossflow Reynolds numbers are defined as $\mathrm{Re}_j = u_j d / \nu_j$ and $\mathrm{Re}_{cf} = u_{cf} d / \nu_{cf}$, respectively, where ν is kinematic viscosity. The jet initial velocity profile is fully-developed turbulent pipe flow. The incoming crossflow is uniform with laminar boundary layer approaching the jet. The boundary layer thickness is measured to be $\delta_{95\%}/d$ = 0.64 at x/d = -2. The velocity fields are measured at 4 cross planes at x/rd = 0.5, 0.75, 1.0, and 1.5.

4. Results

4.1. Volumetric entrainment ratio E

Figure 3 shows the evolution of the entrainment ratio E on rd-scale. Using one-plus-power law in the form of $E = 1 + a_E (x/rd)^{b_E}$, we find

$$E = 1 + 5.12 (x/rd)^{0.52} \qquad R^2 = 0.98\,. \qquad (4)$$

Yuan and Street [5] found the exponent b_E to be approximately 0.7 compared to 0.52 in our case. The two results differ by approximately 30% of the average value between the two. The discrepancy cannot yet be conclusively explained at present. It is noted however that, besides different approaches, the flows in the two works are not at the same condition, especially the effective velocity ratios r are not equal. Our preliminary result as well as Eq. (13) of Yuan and Street show that, in rd-scale, the relation $E(x/rd)$ depends on r.

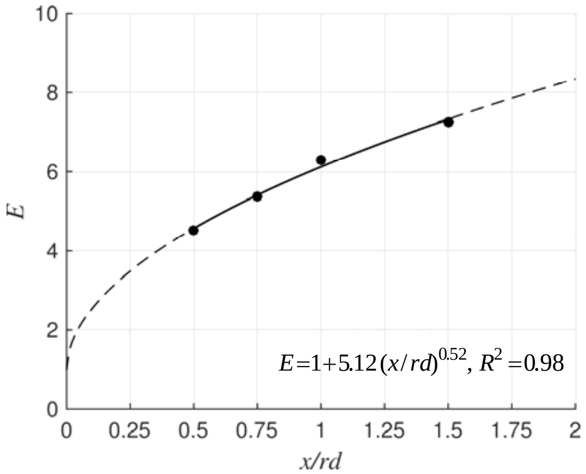

Fig. 3. Evolution of the volumetric entrainment ratio E.

4.2. Scheme for presenting results on structure and entrainment

In the following section, we will present the results on the jet structures, jet-and-crossflow interactions, and entrainment mechanism. In this regard, we first describe the scheme for presenting the graphical results as follows.

Since two seeding schemes are used: (A) jet-fluid only seeding, and (B) jet-and-crossflow fluid seeding, the results must be interpreted differently. In addition, further information can be extracted from the difference (C) = (B)-(A), according to Eq. 2.

The following schemes are used for presenting the results in Figs. 4.1 to 4.3. Each sub-figure in Fig. 4 [(4.1) to (4.3)] corresponds to surface contours of different quantity: (4.1) probability, (4.2) normalized time-mean streamwise velocity, and (4.3) normalized time-mean streamwise vorticity, while each sub-plot [(A) to (C)] in each sub-figure corresponds to the result of different seeding scheme as follows.

Contour surfaces

(A) Jet-fluid only seeding: the result represents the normalized time-mean jet property q_j.

(B) Jet-and-crossflow fluid seeding: the result represents the normalized time-mean field property q.

(C) = (B)-(A): the result represents the approximated normalized time-mean pure crossflow property q_{cf} according to the interpretation and underlying assumptions of Eq. (2).

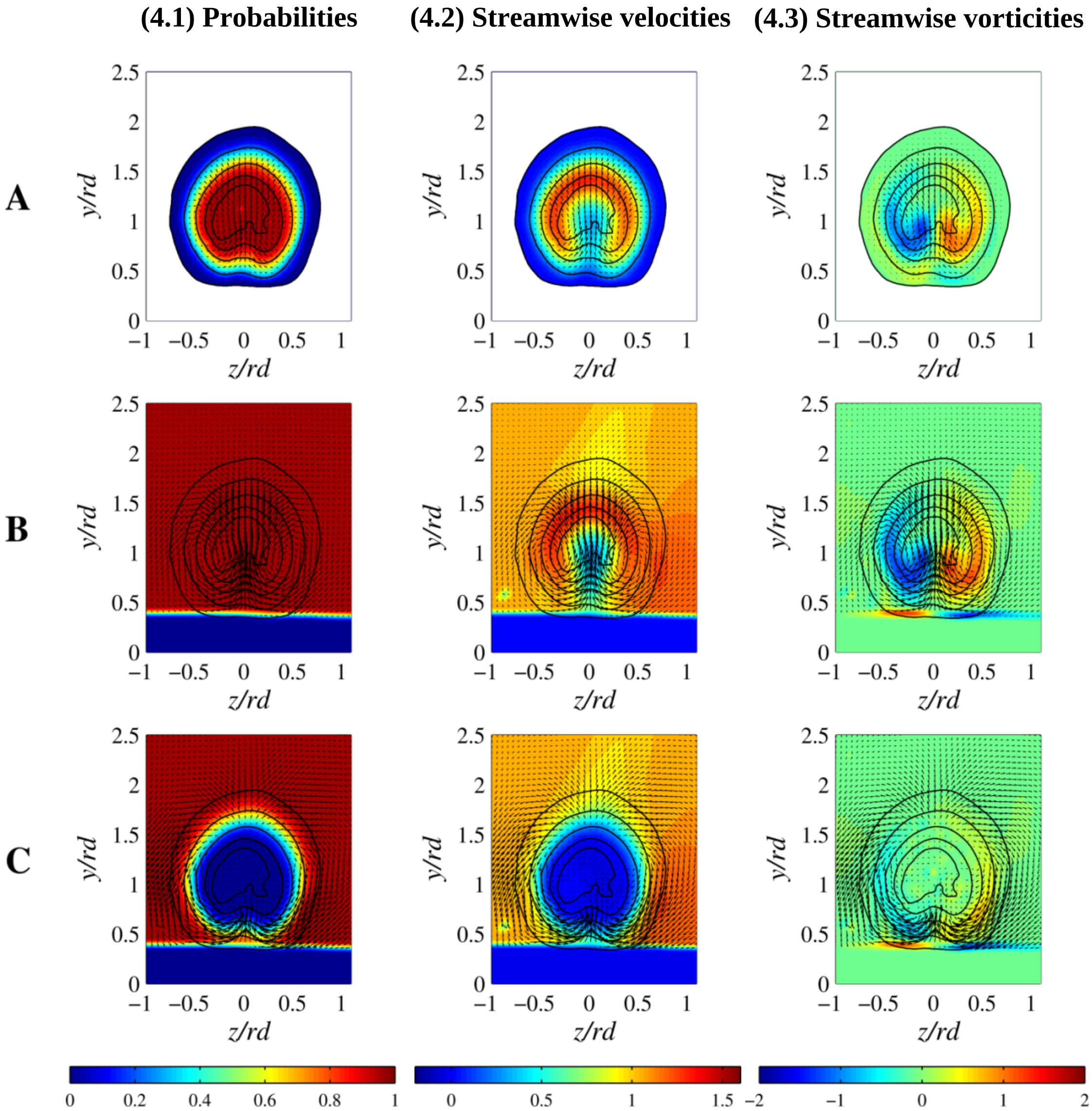

Fig. 4. Normalized time-mean property fields at the cross plane $x/rd = 0.75$.
Surface Contours: (4.1) probability fields,
(4.2) normalized time-mean streamwise velocity fields, and
(4.3) normalized time-mean streamwise vorticity fields.
In-plane vectors: Normalized time-mean in plane vector fields.
Contour lines: Selected values of ϕ_j, from outermost to innermost:

$$\phi_j = 0.01, 0.25, 0.75, 0.95, 0.99.$$

For the sub-plots (A) to (C), see the description in Sec. 4.2.

Furthermore, in order to be able to relate the extent of the jet, the location, the probability of finding jet fluid ϕ_j, and the velocity field among sub-plots more easily, additional contour lines and vector plot are superimposed onto each sub-plot. The scheme for this is as follows.

Contour lines

Selected contour lines of the probability of finding jet fluid ϕ_j will be superimposed on all sub-plots. The selected values of ϕ_j are, from outer to inner, 0.01, 0.25, 0.75, 0.95, 0.99. The reason for these values can be found in Bunyajitradulya [3].

Briefly, they approximately differentiate different regions of the time-mean jet cross section according to their contribution to the total time-mean jet area: being linear in the approximated range of

$$0 < \phi_j / \phi_{j,\max} < 0.01$$

and $$0.25 < \phi_j / \phi_{j,\max} < 0.75 ,$$

where $\phi_{j,\max}$ is the maximum ϕ_j at that cross section, which is typically close to one in the range of parameters investigated.

In-plane vector plot

In-plane velocity vector field will be superimposed on all sub-plots [(A)-(C)]. In this case, all sub-figures [(4.1)-(4.3)] are the same but each subplot [(A)-(C)] has different interpretation as follows.

(A) Normalized time-mean in-plane jet velocity vector $\vec{V}_{j,yz} / u_{cf}$.

(B) Normalized time-mean in-plane field velocity vector $\vec{V}_{yz} / u_{cf}$.

(C) Approximated normalized time-mean in-plane pure crossflow velocity vector $\vec{V}_{cf,yz} / u_{cf}$.

4.3. Structure, jet and crossflow interaction, and entrainment mechanism

As a representative cross plane, the results from the cross plane at x / rd = 0.75 are presented. Qualitatively, the results of other cross planes are similar.

Contour surfaces of Fig. 4.1 shows the probabilities. Figure 4.1(A) shows the timewise probability of finding jet fluid at a point, $\phi_j = N_j / N$. N_j is the total number of instants, or snapshots, at which the SPIV registers non-absolute-zero velocity; in other words, the total number of instants that the PIV tracer particles and by implication the jet-fluid mixture are found. N is the total number of data-acquisition instants. It is seen that ϕ_j is high at the jet center and low and approaches zero at the jet edge. This indicates that, timewise at the jet center the probability of finding the jet-fluid mixture is high while the probability of finding the pure crossflow fluid is low. As we move towards the jet edge, the opposite occurs.

Contour surfaces of Fig. 4.1(B) shows the probability of finding any fluid ϕ , be it the jet-fluid mixture or the pure crossflow fluid. As can be seen, except towards the bottom side close to the wall, ϕ is uniformly and approximately one over the cross plane. This indicates that our crossflow seeding scheme renders the tracer particles to be very - if not ideally - uniform, spatially and temporally.

Contour surfaces of Fig. 4.1(C) shows the probability of finding pure crossflow fluid, ϕ_{cf} . Note that conceptually this is the complement of the probability of finding the jet-fluid mixture, i.e., $\phi_j + \phi_{cf} = \phi = 1$. The reader is however reminded that the results (A) and (B), for which (C) = (A)-(B), come from two different realizations. Similar to Eq. (2), we have the approximation $\phi_{cf,\omega'} \approx \phi_{\omega'} - \phi_{j,\omega}$.

Vector plots in Fig. 4.1 also show the normalized time-mean in-plane velocity fields for (A) the jet velocity $\vec{V}_{j,yz} / u_{cf}$, (B) the field velocity $\vec{V}_{yz} / u_{cf}$ - which exhibits the typical counter-rotating vortex pair (CVP) velocity field, and (C) the pure crossflow velocity $\vec{V}_{cf,yz} / u_{cf}$. Figure 4.1(A) shows the contribution to the typical CVP velocity field from the *jet CVP*, which is more appropriately and clearly identified by the jet streamwise vorticity in Fig. 4.3(A). On the other hand, Fig. 4.1(C) shows its complement, i.e., the contribution to the typical CVP velocity field from the surrounding pure crossflow fluid, whose ‘vortical’ motion is induced by the jet CVP. Note that in Figs. 4.1(A) and (C), which represent the in-plane *jet* (or jet-fluid mixture) and *pure crossflow* velocity fields respectively, we see only each of the ‘half’ of the typical CVP velocity field.

Jet-CVP-induced pure crossflow vortical motion: Starting from Fig. 4.1(C), it can be seen from the in-plane vector plot that the pure crossflow fluid from each lateral side of the jet is being induced by the jet CVP to have a sequence of downward-inward-and-upturn motion. This jet-CVP-induced pure crossflow vortical motion results in the pure crossflow fluid from each lateral side of the jet being brought towards the bell-shaped inlet [of the converging-diverging (C-D) vertical channel of high upward flow] at the bottom edge of the jet. Note that due to the color scheme in Fig. 4.1, the C-D vertical channel of high upward flow can be seen more clearly in Fig. 4.2(B).

Jet-CVP-induced vertical channel of high upward flow, region of intense entrainment: Subsequently, in and through this *converging* section (as opposed to the diverging section) of the vertical channel of high upward flow [Fig. 4.1(B)], the pure crossflow fluid at the bottom edge of the jet below and around the bell-shaped inlet is being entrained continuously and intensely into the jet. The intensity of entrainment in this converging section of the vertical channel (especially towards the inlet end as opposed to the throat end) is such that at the throat of the channel the fluid already becomes mostly the jet-fluid mixture. This can be seen from the level of probability of finding jet fluid ϕ_j which varies in the channel, from low value at the bottom edge of the jet to approaching one ($\phi_j >$ 0.9-0.95) at the throat of the channel. In fact, spatialwise, considering the gradient of ϕ_j, the region of intense entrainment can be approximately identified as in the region $0.25 < \phi_j < 0.75$, which approximately coincides towards the inlet end of the converging section of the channel.

From the contour surfaces of the streamwise jet velocity [Fig. 4.2(A)] as well as of the streamwise field velocity [Fig. 4.2(B)], it is noted that the major portion of the C-D vertical channel is in the low streamwise jet and field velocity region compared to the surrounding lateral and top region of higher streamwise jet and field velocity. For clarity, we shall identify and refer to the region of *high streamwise jet velocity*, which is of kidney-shaped [Fig. 4.2(A)], as the *jet kidney-shaped structure*. In addition, below the jet kidney-shaped structure, there is a gulf region of low streamwise jet velocity. We shall identify and refer to this region of *low streamwise jet velocity*, which is of a gulf-shaped [Fig. 4.2(A)], as the *gulf* region (of the jet kidney-shaped structure). As we shall later see, this jet kidney-shaped structure and its gulf region play dominant role in the following and final stage of entrainment. Finally, it is noted that the throat of the vertical channel of high upward flow, at which the fluid is now mostly the jet-fluid mixture, is approximately at the center of the gulf [Fig. 4.2(A) or (B)].

Free-jet like entrainment by the jet kidney-shaped structure: What was pure crossflow fluid at the bottom edge of the jet below and around the bell-shaped inlet is now entrained and already becomes mostly the jet-fluid mixture in the gulf. The low streamwise velocity jet-fluid mixture in the gulf is subsequently entrained into the high streamwise jet velocity region of the jet kidney-shaped structure that lies above and surrounds it, similar to free-jet entrainment.

In order to identify the jet CVP more clearly and to confirm its role in entrainment mechanism

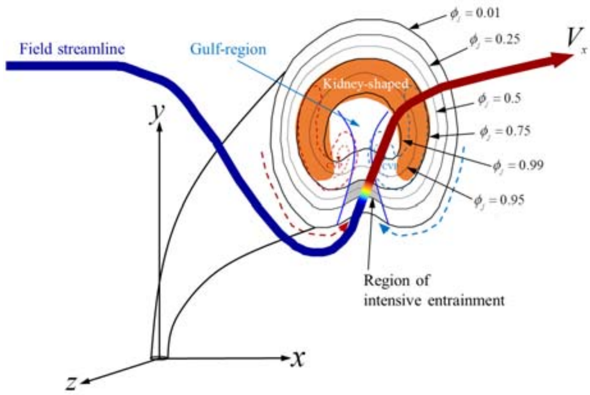

Fig. 5. A sketch qualitatively illustrates the cross-plane entrainment mechanism of a jet in crossflow. The streamline drawn represents the field streamline while the color shading of the field streamline represents the probability of finding jet fluid ϕ_j, blue being towards zero and red being towards one.

described above, we plot the normalized time-mean streamwise vorticity in Fig. 4.3: (A) jet vorticity, $\omega_{j,x} d / u_{cf}$, in which the *jet-CVP* is here identified, (B) field vorticity, $\omega_x d / u_{cf}$, and (C) pure crossflow vorticity, $\omega_{cf,x} d / u_{cf}$. It is evident in this figure that the pure crossflow vortical motion as well as the converging-diverging vertical channel of high upward flow is induced by the jet CVP, which is in the form of a pair of 'inverse commas' [Fig. 4.3(A)].

Finally, we summarize the entrainment mechanism described above as a sketch in Fig. 5. The entrainment mechanism described above is qualitatively similar to that described by Cortelezzi and Karagozian [7].

5. Conclusions

Structures, jet-and-crossflow interactions, entrainment, and cross-plane entrainment mechanism of a jet in crossflow are investigated.

The results show that, in the cross-plane the jet CVP, the dominant jet counter-rotating vortex pair of 'inverse comma' shape, dominates the flow and entrainment mechanism. Specifically, the cross-plane entrainment mechanism can be described in three subsequent stages as follows.

1. **Jet-CVP-induced pure crossflow vortical motion**: In this early stage, the jet-CVP induces the downward-inward-and-upturn motion of the surrounding pure crossflow fluid.

This results in the induction of the pure crossflow fluid from each lateral side of the jet towards the bell-shaped inlet of the converging-diverging vertical channel of high upward flow at the bottom edge of the jet.

2. **Jet-CVP-induced vertical channel of high upward flow**: This stage subsequently brings the pure crossflow fluid from the bottom edge of the jet below and around the bell-shaped inlet through the converging section of the vertical channel. The existence of this vertical channel is induced and fueled by the jet CVP. In the converging section of the channel, especially towards the inlet end (as opposed to the throat end), the pure crossflow fluid is being entrained continuously but intensely such that, when the fluid reaches the throat of the channel at the center of the gulf of the jet kidney-shaped structure, it already becomes mostly the jet-fluid mixture.

3. **Free-jet like entrainment by the jet kidney-shaped structure**: The jet kidney-shaped structure of high streamwise jet velocity subsequently entrains the jet-fluid mixture in the gulf region of low streamwise jet velocity into itself.

The entrainment mechanism is illustrated as a sketch in Fig. 5.

6. Acknowledgements

Thai Government Research Fund for the fiscal years 2557: Contract No. GRB_APS_23_57_21_01 is gratefully acknowledged. We are thankful for the suggestions and assistances of Mr. Apichet Srimekharat, Mr. Kittikun Wongthongsiri, Mr. Settasit Chaikasetsin, Mr. Suphak Dawyok. We also appreciate the assistances and the cooperations of Mr. Pattarapol Suppamongkol, Mr. Chaowat Tekhuad, Mr. Anand Kulpiyavaja, Mr. Apiwat Chaninwongsiri, Ms. Minthanon Chairat, Mr. Saran Wangkiat, Mr. Sumate Khemakanon and Mr. Apichote Kengkarnpanich.

7. References

[1] Witayaprapakorn, T. and Bunyajitradulya, A. (2013). Effects of azimuthal control jets on structure and entrainment of a jet in crossflow, paper presented in *The Twenty-Seventh Conference of the Mechanical Engineering Network of Thailand*, October 16 – 18, 2013, Chonburi, Thailand.

[2] Chaikasetsin, S., Sushewakhul, T., Panusittikorn, P. and Bunyajitradulya, A. (2014). Effects of Azimuthal Control Jets to Main Jet Mass Flowrate Ratio on the Entrainment of a Jet in Crossflow, paper presented in *The 5th TSME International Conference on Mechanical Engineering*, December 17-19, 2014, Chiang Mai, Thailand.

[3] Bunyajitradulya, A. (2015). Evaluation of the volumetric entrainment ratio of a jet in crossflow and its evolution, Thai Government GRB_APS_23_57_21_01 Research Project Report, *Thai Government Research Fund FY 2557*.

[4] Wangkiat, S., Khemakanon, S., Kengkarnpanich, A., and Bunyajitradulya, A. (2015). Effects of the azimuthal positions of the azimuthal control jets on structures and entrainment of a jet in crossflow at high effective velocity ratio 12, paper presented in *The 6th TSME International Conference on Mechanical Engineering*, Cha-Am, Phetchaburi, Thailand.

[5] Yuan, L.L. and Street, R.L. (1998). Trajectory and entrainment of a round jet in crossflow, *Phys. Fluids*, vol. 10, no. 9, pp. 2323-2335.

[6] Yuan, L.L., Street, R.L., and Ferziger, J.H. (1999). Large-eddy simulation of a round jet in crossflow, *J. Fluid Mech.*, vol. 379, pp. 71-104.

[7] Cortelezzi, L. and Karagozian, A.R. (2001). On the formation of the conter-rotating vortex pair in traverse jets, *J.Fluid Mech.*, vol.446, pp. 347-373.

[8] Sau, A., Sheu, T.W.H., Hwang, R.R., and Yang, W.C. (2004). Three-dimensional simulation of square jets in cross-flow, *Phys Rev*, vol.69.